Photon Pressure with an Effective Negative Mass Microwave Mode

I. C. Rodrigues,[1,2,*] G. A. Steele,[1,†] and D. Bothner[3,1,‡]
[1]Kavli Institute of Nanoscience, Delft University of Technology, PO Box 5046, 2600 GA Delft, The Netherlands
[2]Department of Physics, ETH Zürich, Zürich, Switzerland
[3]Physikalisches Institut, Center for Quantum Science (CQ) and LISA+, Universität Tübingen, 72076 Tübingen, Germany

(Received 11 December 2022; revised 11 March 2024; accepted 25 March 2024; published 17 May 2024)

Harmonic oscillators belong to the most fundamental concepts in physics and are central to many current research fields such as circuit QED, cavity optomechanics, and photon pressure systems. Here, we engineer a microwave mode in a superconducting LC circuit that mimics the dynamics of a negative mass oscillator, and couple it via photon pressure to a second low-frequency circuit. We demonstrate that the effective negative mass dynamics lead to an inversion of dynamical backaction and to sideband cooling of the low-frequency circuit by a blue-detuned pump field, which can be intuitively understood by the inverted energy ladder of a negative mass oscillator.

DOI: 10.1103/PhysRevLett.132.203603

The harmonic oscillator (HO) is one of the most fundamental models in physics and can be used to describe many kinds of systems, most prominently mechanical oscillators and electrical resonant circuits, but also optical cavities, acoustic crystal vibrations, or collective spin oscillations in magnets. HOs also play a crucial role for the development of quantum technologies, of which some of the most relevant are circuit quantum electrodynamics (cQED) [1,2] and cavity optomechanics [3,4] as well as its cQED equivalent, photon pressure systems [5–7]. In nearly all experimental cases HOs have a positive "mass" (positive capacitance in LC circuits). Note that we use the term "mass" in a generalized sense, i.e., for any quantity that describes the inertia of the HO. However, in addition to theoretical considerations [8–13] there have been experimental reports of effective negative mass HOs realized through spin ensembles [14–17], through the common modes of two micromechanical oscillators [18], and in multimode electromechanical systems [19]. In these works, the negative mass has fascinating practical consequences such as providing quantum-mechanics-free or backaction-free subspaces [11] and enabling entanglement between distinct oscillators [14,18]. Despite these promising perspectives, it is very challenging to experimentally realize negative effective mass oscillators, and new approaches are under investigation [20].

Here, we present a simple method to create an effective negative mass HO which only requires a Kerr nonlinearity and is therefore not limited to specific platforms. The effective negative mass HO is prepared by strongly driving a weakly nonlinear superconducting LC circuit, which leads to a susceptibility inversion compared to the positive mass case. Similar driving schemes in nonlinear systems have lately been implemented with both LC circuits and mechanical oscillators [21,22], but it has not been demonstrated yet that such an approach creates a dynamically stabilized analog of a negative mass mode. The integration of this mode into a photon pressure device allows us to use the interaction with a low-frequency (LF) circuit as a probe for the effective mode mass through dynamical backaction. Most strikingly, we find that dynamical backaction effects get inverted compared to positive mass modes, which leads to sideband cooling of the LF circuit by a blue-detuned pump field.

To explore the (classical) phenomenology of a negative mass HO, we consider the susceptibility $\chi_m(\omega)$, which describes the response of a low-loss mechanical oscillator with mass m to an external excitation $F_{\mathrm{ex}}(\omega)$ in frequency space

$$\chi_m(\omega) = \frac{1}{2m\omega_0}\frac{1}{\frac{\kappa}{2} + i(\omega - \omega_0)}, \tag{1}$$

i.e., $x(\omega) = -i\chi_m(\omega)F_{\mathrm{ex}}(\omega)$. Here, ω is the excitation frequency, ω_0 is the resonance frequency, and κ is the oscillator decay rate. With a negative mass, however, one obtains a HO with a susceptibility $\chi_-(\omega) = -\chi_+(\omega)$, where $\chi_+(\omega)$ is the susceptibility of a positive mass oscillator [23]. At first glance, this may not look particularly striking, as it introduces only a phase shift of π compared to a positive mass oscillator, but it is the essence of an effective negative mass [23]. Below, we will demonstrate that integrating such an inverted susceptibility oscillator and its corresponding phase-shifted response into a system of photon pressure circuits leads to dramatic consequences in the interaction of the two circuits.

Before we dive into the details of our experiment, we introduce a suceptibility expression for a more general HO:

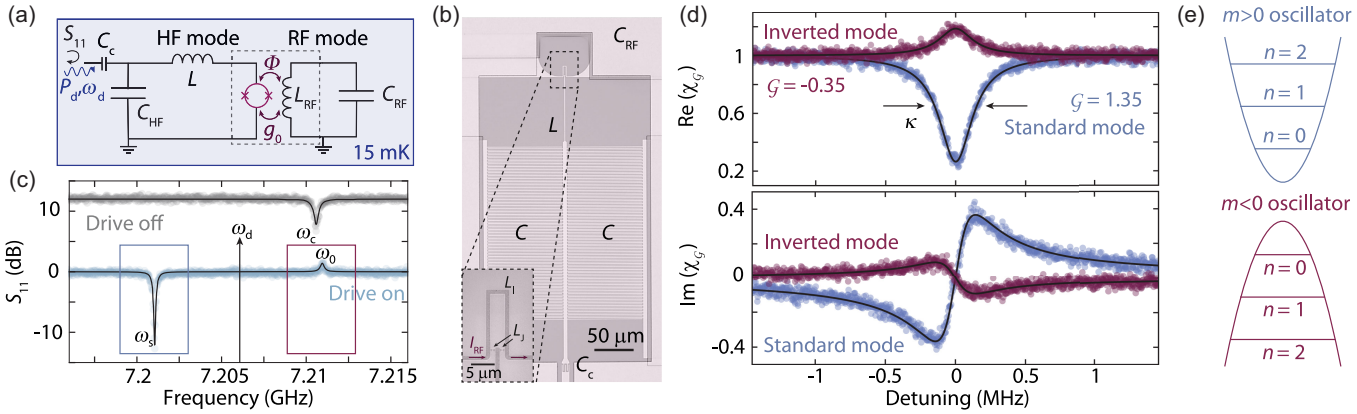

FIG. 1. Engineering an effective negative mass microwave mode in a strongly driven photon pressure circuit. (a) Circuit schematic. Linear inductances and capacitances are L, $C_{\mathrm{HF}} = 2C$, L_{RF}, C_{RF}, the single-photon coupling rate is g_0, and the HF mode is coupled to a feedline by means of a coupling capacitance C_{c}. The HF circuit is driven with a strong, near-resonant tone at ω_{d} and with power P_{d}, and simultaneously the reflection response $S_{11}(\omega)$ is tracked with a small probe signal. (b) Images of the device. Bright parts are aluminum, dark and transparent parts are silicon. Inset: scanning electron microscopy (SEM) image of the coupling region. Junctions are labeled with L_{J}, loop inductance by L_{l}, and the RF mode current is indicated by I_{RF}. In the SEM image darker parts are Al, brighter parts Si. (c) Reflection S_{11} both without and with strong drive in direct comparison; lines are fits. Undriven curve is offset by $+12$ dB. The undriven resonance frequency is ω_{c}, and the driven response shows two modes at ω_{s} and ω_0. (d) Real and imaginary parts of the mode susceptibilities $\chi_{\mathcal{G}}$ of the two modes at ω_{s} and ω_0 vs their corresponding detunings Δ_0, Δ_{s}. Lines are fits with Eq. (2). (e) Potential and energy levels of a positive mass ($\mathcal{G} > 0$, top) and a negative mass ($\mathcal{G} < 0$, bottom) HO.

$$\chi_{\mathcal{G}}(\omega) = \frac{\mathcal{G}}{\frac{\kappa}{2} + i(\omega - \omega_0)}. \tag{2}$$

Here, we have chosen a convention without the prefactor $1/(2m\omega_0)$ of Eq. (1), but added a dimensionless parameter $\mathcal{G}$ in the numerator, which becomes negative for a negative mass oscillator. The case $\mathcal{G} > 1$ represents intracavity amplification, recently considered in Ref. [24], and here we explore the implications of $\mathcal{G} < 0$.

Our device combines a superconducting radio-frequency (RF) circuit with a high-frequency (HF) quantum interference circuit, which are coupled to each other via a magnetic flux-tunable photon pressure interaction, cf. Figs. 1(a), 1(b) and Refs. [24,25]. The RF circuit has a resonance frequency $\Omega_0 = 2\pi \times 452$ MHz and a linewidth $\Gamma_0 = 2\pi \times 45$ kHz. The undriven HF cavity has a resonance frequency of $\omega_{\mathrm{c}} = 2\pi \times 7.211$ GHz, and a total (external) linewidth of $\kappa = 2\pi \times 420$ kHz ($\kappa_{\mathrm{e}} = 2\pi \times 78$ kHz). We flux bias the device at an operation point with a single-photon coupling rate $g_0 = 2\pi \times 175$ kHz and an HF cavity Kerr constant $\mathcal{K} = -2\pi \times 6.6$ kHz, which originates from the integrated constriction-type Josephson junctions. All experiments have been conducted in a dilution refrigerator at a base temperature of $T_{\mathrm{b}} \approx 15$ mK. More details can be found in Refs. [24,25].

Without any particular measures, the HF cavity displays $\mathcal{G} = 1$. To obtain $\mathcal{G} < 0$ we use the HF mode Kerr nonlinearity. A strong near-resonant drive tone leads to the appearance of two quasimodes in the probe response of the system [21,26]. The response of one of the modes is equivalent to $\mathcal{G} > 1$ (the signal mode at ω_{s}), and the second mode shows $\mathcal{G} < 0$ (the idler mode at ω_0); cf. Fig. 1(c), (d). The idler mode is closely related to Bogoliubov ghost branches observed in condensates and quantum fluids [27–31], and so another suitable name for it would be ghost mode. The origin of this double-mode response is four-wave mixing and parametric amplification [21]. The probe reflection near ω_0 is given by

$$S_{11}(\omega \approx \omega_0) = 1 - \kappa_{\mathrm{e}}\chi_{\mathcal{G}} = 1 - \frac{\kappa_{\mathrm{e}}\mathcal{G}}{\frac{\kappa}{2} + i(\omega - \omega_0)} \tag{3}$$

with $\mathcal{G} = -0.35$, $\kappa = 2\pi \times 290$ kHz, and $\omega_0 = 2\pi \times 7.211$ GHz (the smaller κ compared to the undriven case is most likely related to saturation of two-level systems by the drive [24,32]). Although both $\mathcal{G} > 1$ and $\mathcal{G} < 0$ can lead to a resonance peak in the reflection response, the interpretation behind it is fundamentally different. For $\mathcal{G} > 1$ the peak arises from amplification of the intracavity field, for $\mathcal{G} < 0$ from a phase shift of π, which is equivalent to a negative mass HO [23].

The negative-mass-inverted susceptibility, however, is not limited to an apparent effect in the reflection response to a probe tone. Sideband fields from an additional photon pressure pump tone will also experience the effective inversion. In the following we will consider the driven system with an additional photon pressure pump tone applied at the blue idler-mode sideband $\omega_{\mathrm{p}} = \omega_0 + \Omega_0$; cf. Fig. 2(a). We will also work in a reduced HF mode space, where all we consider is a single generalized mode with $\mathcal{G} < 0$. The linearized and approximated equations of motion in Fourier space for the intracavity field fluctuation $\hat{c}$, $\hat{c}^\dagger$ and the RF mode amplitude $\hat{b}$, $\hat{b}^\dagger$ ladder operators then are [23,24]

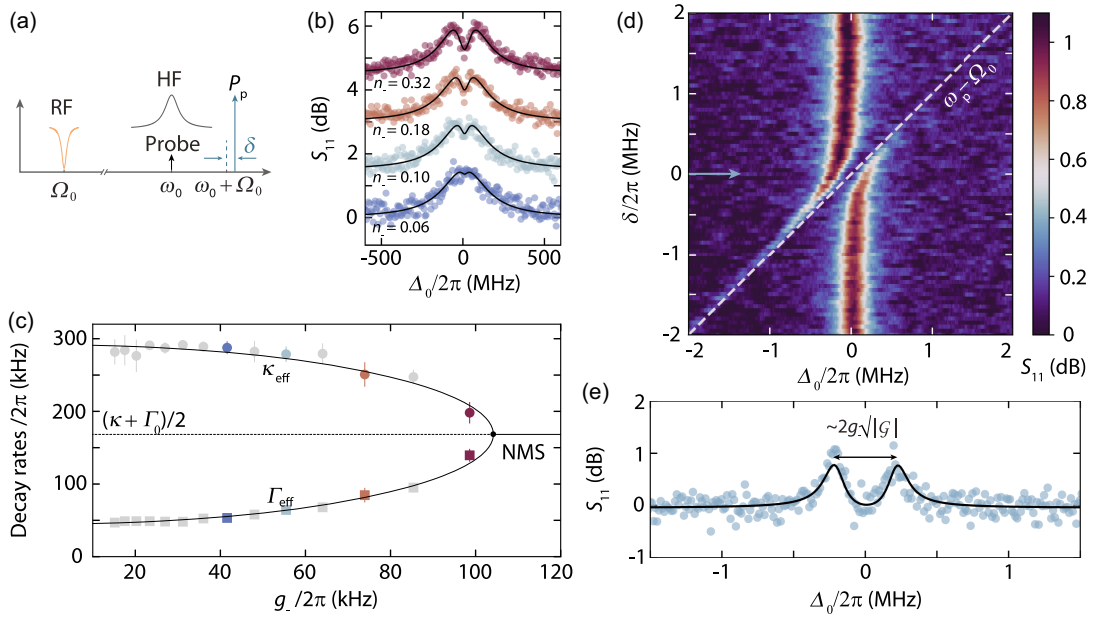

FIG. 2. Dynamical backaction inversion and normal-mode splitting with an effective negative mass microwave mode. (a) Schematic of the experiment. A pump tone (power P_p) is applied at $\omega_p = \omega_0 + \Omega_0 + \delta$. A small probe field tracks S_{11} around ω_0. (b) S_{11} vs $\Delta_0 = \omega - \omega_0$ for different P_p and $\delta = 0$. The cavity resonance peak displays photon pressure induced absorption, an interference effect equivalent to optomechanically induced absorption. From the fits (lines), we obtain Γ_{eff} and κ_{eff}, respectively, which are plotted in panel (c) vs $g_- = \sqrt{n_-}g_0$ with n_- the intracavity pump photon number. Details can be found in the Supplemental Material [23]. Symbols are data, and lines are following Eq. (7). The onset of normal-mode splitting is labeled with NMS. (d) S_{11} vs $\Delta_0 = \omega - \omega_0$ and δ. The arrow indicates the linescan shown in (e). The splitting between the modes for $\delta = 0$ is $\sim 2\sqrt{|\mathcal{G}|}|g_-| \approx 2\pi \times 500$ kHz $> \kappa, \Gamma_0$ and indicates the strong-coupling regime. For panels (d) and (e) the HF cavity was driven with slightly different parameters and $\mathcal{G} = -0.21$ [23].

$$\frac{\hat{c}}{\chi_{\mathcal{G}}} = -ig_-\hat{b}^\dagger + \sqrt{\kappa_e}\hat{\xi}_{e,\mathrm{eff}} + \sqrt{\kappa_i}\hat{\xi}_{i,\mathrm{eff}} \tag{4}$$

$$\frac{\hat{b}^\dagger}{\bar{\chi}_0} = ig_-^*\hat{c} + \sqrt{\Gamma_e}\hat{\zeta}_e^\dagger + \sqrt{\Gamma_i}\hat{\zeta}_i^\dagger, \tag{5}$$

where $\bar{\chi}_0^{-1} = \Gamma_0/2 + i(\Omega + \Omega_0)$ is the RF mode susceptibility, $\Omega = \omega - \omega_p$ is the frequency relative to the pump tone, κ_e, κ_i and Γ_e, Γ_i are the external and internal coupling rates of the circuits to their corresponding baths, and $\hat{\zeta}_{e,i}$ are the noise input operators for the RF mode following $\langle\hat{\zeta}_{e,i}^\dagger\hat{\zeta}_{e,i}\rangle = n_{e,i}^{RF}$. The multiphoton coupling rate is $g_- = \gamma_- g_0$ with the sideband pump intracavity amplitude γ_-, related to the intracavity pump photon number n_- through $n_- = |\gamma_-|^2$ [33].

We combine Eqs. (4) and (5) to find the effective RF mode susceptibility, and what we get looks formally identical to the usual blue sideband pumped system with

$$\bar{\chi}_0^{\mathrm{eff}}(\Omega) = \frac{1}{\frac{\Gamma_0}{2} + i(\Omega + \Omega_0) - |g_-|^2\chi_{\mathcal{G}}(\Omega)}. \tag{6}$$

When pumping exactly on the blue sideband, the complex eigenfrequencies $\tilde{\Omega}_\pm$ of this susceptibility are given by

$$\tilde{\Omega}_\pm = -\Omega_0 + i\frac{\kappa+\Gamma_0}{4} \pm i\sqrt{\left[\frac{\kappa-\Gamma_0}{4}\right]^2 + \mathcal{G}|g_-|^2}, \tag{7}$$

obtained through the condition $\chi_0^{\mathrm{eff}}(\tilde{\Omega})^{-1} = 0$.

As long as the coupling is not too large $[(\kappa-\Gamma_0)/4]^2 > -\mathcal{G}|g_-|^2$, the expression under the root will be > 0, and the two modes (RF and HF) will just display modified linewidths Γ_{eff} and κ_{eff} given by $2\mathrm{Im}(\tilde{\Omega}_\pm)$. Hence, the effective RF linewidth Γ_{eff} will indeed increase with increasing $|g_-|$ in the case that $\mathcal{G} < 0$; we obtain blue-sideband-pumped positive dynamical backaction damping. The result is also in excellent quantitative agreement with the experimental data; cf. Fig. 2. The phase shift of π in the susceptibility implies that for a blue-detuned pump the intracavity field is not adjusting in a way which amplifies the RF oscillation as in a regular cavity, but in a way that opposes the RF "motion" and is therefore reducing its amplitude.

For even stronger pumping $-\mathcal{G}|g_-|^2 > [(\kappa-\Gamma_0)/4]^2$ the square root in Eq. (7) becomes imaginary, and we find two distinct resonance frequency solutions with identical damping rates $(\kappa+\Gamma_0)/2$. We witness the onset of normal-mode splitting, and for slightly larger $|g_-|$ even the onset of the strong-coupling regime [7,34,35] [splitting larger than $(\kappa+\Gamma_0)/2$], cf. Figs. 2(d) and 2(e), which is something that could not happen with $\mathcal{G} > 0$ for blue-detuned pumping.

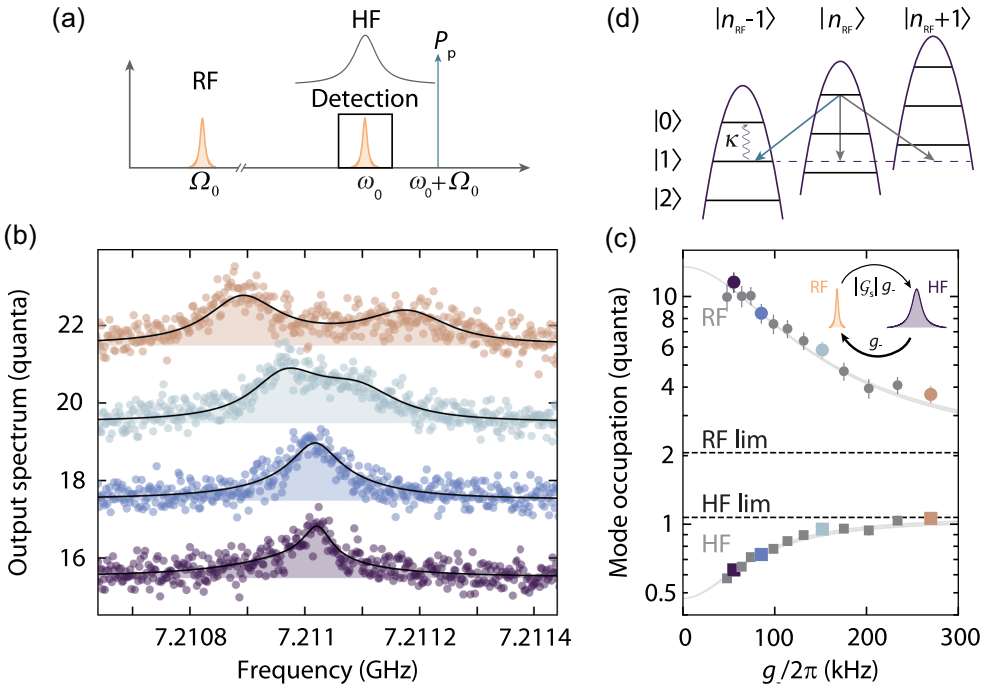

FIG. 3. Blue-detuned photon pressure sideband cooling with an effective negative mass microwave reservoir. (a) Schematic of the experiment. A pump tone with power P_p is applied at $\omega_p = \omega_0 + \Omega_0$. The HF mode output PSD is recorded for each P_p with a spectrum analyzer. (b) HF mode PSD in units of quanta for various P_p, curves are offset manually by $+2$ each (lowest curve unshifted). Circles are data; lines and shaded areas are fits. From the fits we extract the occupation of both modes n_{fin}^{RF} and n_{fin}^{HF}. The result is plotted in panel (c) vs g_-, circles are data, gray lines are theory including uncertainties [23]. Owing to $|\mathcal{G}| < 1$, we also observe an imbalance in the final mode occupations $n_{lim}^{RF} > n_{lim}^{HF}$, which is related to nonreciprocal heat flow [24]. The two horizontal dashed lines show the limit values for the RF and HF occupations for $g_- \gg \kappa, \Gamma_0$. Error bars in the data points consider the standard deviation of n_{th}^{RF} and the fitting error of each PSD [23]. (d) Energy level schematic of the effective photon scattering process that leads to blue-detuned RF mode cooling.

Finally, we demonstrate that the inverted dynamical backaction also leads to blue-detuned sideband cooling of the RF mode. For this experiment, we put again a pump to the blue sideband of the negative mass HF mode and detect the HF mode output noise with a spectrum analyzer; cf. Fig. 3(a). From the observed power spectral density (PSD), cf. Fig. 3(b), we can infer the occupation of both, the HF mode and the RF mode by fitting the PSD in units of quanta [23]. For this, we assume the unpumped thermal occupation of the HF mode to be negligible. The result reveals that indeed the RF mode is sideband cooled by the blue-detuned pump tone; cf. Figs. 3(c) and 3(d). The starting residual occupation is $n_{th}^{RF} \sim 13.5$, and the cooling reduces this to $n_{fin}^{RF} \sim 3.5$. At the same time, the effective HF mode occupation is increased from its effective occupation without the cooling tone $\tilde{n}_{th}^{HF} \sim 0.5$ to $n_{fin}^{HF} \sim 1$. For the limit $g_- \to \infty$ we get $n_{lim}^{RF} > n_{lim}^{HF}$ and not $n_{lim}^{RF} = n_{lim}^{HF}$ as expected for standard photon pressure and optomechanical systems [25,36,37]. The reason behind this asymmetry is nonreciprocal heat transfer due to $|\mathcal{G}| \neq 1$ as also discussed in Ref. [24].

There is a simple level-diagram interpretation of this blue-detuned cooling with an effective negative mass reservoir. In a negative mass mode adding one excitation corresponds to lowering the energy by $\hbar\omega_0$ [8]. The sideband transition $|n_{HF}, n_{RF}\rangle \to |n_{HF}+1, n_{RF}-1\rangle$, which leads to cooling of the RF mode, has the energy $\hbar(\omega_0 + \Omega_0)$ [cf. Fig. 3(d)], which corresponds to a blue-detuned sideband photon. In that sense, the blue-detuned cooling actually serves as a probe for the sign of the effective oscillator mass. With a positive mass the blue-detuned pump would correspond to a two-mode-squeezing (TMS) interaction and amplification instead of cooling, since the down-scattered photons from the HF pump would lose $\hbar\Omega_0$, and that energy would be added to the RF mode [38]. With a negative mass, creation and annihilation operators in a sense swap roles, and the usual TMS interaction is converted to a beam-splitter term. Finally, we also note that the effect we report here is different from the seemingly similar effect reported recently in an optomechanical system [39], where the blue-detuned cooling is a consequence of the interference of many mechanical sidebands, while here it is a single sideband effect.

In conclusion, we have reported the engineering of an effective negative mass HO in a microwave LC circuit and demonstrated its effect to the photon pressure coupling between this cavity and a radio-frequency LC circuit. The effective negative-mass dynamics emerged from a

combination of a Kerr nonlinearity and strong driving, a method compatible with all kinds of nonlinear oscillators. We found that a blue-detuned sideband pump field leads to positive dynamical backaction damping, normal-mode splitting, and sideband cooling, all things usually associated with red-detuned pumping and a beam-splitter interaction [37,40–42]. Our results demonstrate how to mimic an effective negative mass mode in a generic Kerr oscillator.

All data presented in this paper and the corresponding processing scripts used during the analysis are available on Zenodo [43].

This research was supported by the Netherlands Organisation for Scientific Research (NWO) in the Innovational Research Incentives Scheme—VIDI, Project No. 680-47-526. This project has received funding from the European Research Council (ERC) under the European Union's Horizon 2020 research and innovation program (Grant Agreement No. 681476—QOMD), from the European Union's Horizon 2020 research and innovation program (Grant Agreement No. 732894—HOT), from the Deutsche Forschungsgemeinschaft (DFG, German Research Foundation) via Grant No. 490939971 (BO 6068/1-1).

*icorveira@phys.ethz.ch
†g.a.steele@tudelft.nl
‡daniel.bothner@uni-tuebingen.de

[1] J. Q. You and Franco Nori, Atomic physics and quantum optics using superconducting circuits, Nature (London) **474**, 589 (2011).
[2] A. Blais, A. L. Grimsmo, S. M. Girvin, and A. Wallraff, Circuit quantum electrodynamics, Rev. Mod. Phys. **93**, 025005 (2021).
[3] M. Aspelmeyer, T. J. Kippenberg, and F. Marquardt, Cavity optomechanics, Rev. Mod. Phys. **86**, 1391 (2014).
[4] S. Barzanjeh, A. Xuereb, S. Gröblacher, M. Paternostro, C. A. Regal, and E. M. Weig, Optomechanics for quantum technologies, Nat. Phys. **18**, 15 (2022).
[5] J. R. Johansson, G. Johansson, and F. Nori, Optomechanical-like coupling between superconducting resonators, Phys. Rev. A **90**, 053833 (2014).
[6] C. Eichler and J. R. Petta, Realizing a circuit analog of an optomechanical system with longitudinally coupled superconducting resonators, Phys. Rev. Lett. **120**, 227702 (2018).
[7] D. Bothner, I. C. Rodrigues, and G. A. Steele, Photon pressure strong coupling between two superconducting circuits, Nat. Phys. **17**, 85 (2021).
[8] R. J. Glauber, Amplifiers, attenuators, and Schrödinger's cat, Ann. N.Y. Acad. Sci. **480**, 336 (1986).
[9] K. Hammerer, M. Aspelmeyer, E. S. Polzik, and P. Zoller, Establishing Einstein-Podolsky-Rosen channels between nanomechanics and atomic ensembles, Phys. Rev. Lett. **102**, 020501 (2009).
[10] M. Tsang and C. M. Caves, Coherent quantum-noise cancellation for optomechanical sensors, Phys. Rev. Lett. **105**, 123601 (2010).
[11] M. Tsang and C. M. Caves, Evading quantum mechanics: Engineering a classical subsystem within a quantum environment, Phys. Rev. X **2**, 031016 (2012).
[12] K. Zhang, P. Meystre, and W. Zhang, Back-action-free quantum optomechanics with negative-mass Bose-Einstein condensates, Phys. Rev. A **88**, 043632 (2013).
[13] A. Motazedifard, F. Bemani, M. H. Naderi, R. Roknizadeh, and D. Vitali, Force sensing based on coherent quantum noise cancellation in a hybrid optomechanical cavity with squeezed-vacuum injection, New J. Phys. **18**, 073040 (2016).
[14] B. Julsgaard, A. Kozhekin, and E. S. Polzik, Experimental long-lived entanglement of two macroscopic objects, Nature (London) **413**, 400 (2001).
[15] W. Wasilewski, K. Jensen, H. Krauter, J. J. Renema, M. V. Balabas, and E. S. Polzik, Quantum noise limited and entanglement-assisted magnetometry, Phys. Rev. Lett. **104**, 133601 (2010).
[16] C. B. Møller, R. A. Thomas, G. Vasilakis, E. Zeuthen, Y. Tsaturyan, M. Balabas, K. Jensen, A. Schliesser, K. Hammerer, and E. S. Polzik, Quantum back-action-evading measurement of motion in a negative mass reference frame, Nature (London) **547**, 191 (2017).
[17] J. Kohler, J. A. Gerber, E. Dowd, and D. M. Stamper-Kurn, Negative-mass instability of the spin and motion of an atomic gas driven by optical cavity backaction, Phys. Rev. Lett. **120**, 013601 (2018).
[18] L. M. de Lepinay, C. F. Ockeloen-Korppi, M. J. Woolley, and M. A. Sillanpää, Quantum mechanics-free subsystem with mechanical oscillators, Science **372**, 625 (2021).
[19] N. R. Bernier, L. D. Tóth, A. K. Feofanov, and T. J. Kippenberg, Level attraction in a microwave optomechanical circuit, Phys. Rev. A **98**, 023841 (2018).
[20] J. Junker, D. Wilken, N. Johny, D. Steinmeyer, and M. Heurs, Frequency-dependent squeezing from a detuned squeezer, Phys. Rev. Lett. **129**, 033602 (2022).
[21] F. Fani Sani, I. C. Rodrigues, D. Bothner, and G. A. Steele, Level attraction and idler resonance in a strongly driven Josephson cavity, Phys. Rev. Res. **3**, 043111 (2021).
[22] J. S. Huber, G. Rastelli, M. J. Seitner, J. Kölbl, W. Belzig, M. I. Dykman, and E. M. Weig, Spectral evidence of squeezing of a weakly damped driven nanomechanical mode, Phys. Rev. X **10**, 021066 (2020).
[23] See Supplemental Material at http://link.aps.org/supplemental/10.1103/PhysRevLett.132.203603 contains a general theoretical discussion of negative mass oscillators and negative capacitance LC circuits, a detailed theoretical treatment of the specific experiment presented here, additional data, details on the data analysis and the calculation of the error bars.
[24] I. C. Rodrigues, G. A. Steele, and D. Bothner, Parametrically enhanced interactions and nonreciprocal bath dynamics in a photon pressure Kerr amplifier, Sci. Adv. **87**, eabq1690 (2022).
[25] I. C. Rodrigues, D. Bothner, and G. A. Steele, Cooling photon pressure circuits into the quantum regime, Sci. Adv. **7**, eabg6653 (2021).

[26] J. S. Ochs, M. Seitner, M. I. Dykman, and E. M. Weig, Amplification and spectral evidence of squeezing in the response of a strongly driven nanoresonator to a probe field, Phys. Rev. A **103**, 013506 (2021).
[27] C. Ciuti, P. Schwendimann, and A. Quattropani, Parametric luminescence of microcavity polaritons, Phys. Rev. B **63**, 041303(R) (2001).
[28] J. M. Vogels, K. Xu, C. Raman, J. R. Abo-Shaeer, and W. Ketterle, Experimental observation of the Bogoliubov transformation for a Bose-Einstein condensed gas, Phys. Rev. Lett. **88**, 060402 (2002).
[29] V. Kohnle, Y. Léger, M. Wouters, M. Richard, M. T. Portella-Oberli, and B. Deveaud-Plédran, From single particle to superfluid excitations in a dissipative polariton gas, Phys. Rev. Lett. **106**, 255302 (2011).
[30] M. Pieczarka, M. Syperek, L. Dusanowski, J. Misiewicz, F. Langer, A. Forchel, M. Kamp, C. Schneider, S. Höfling, A. Kavokin, and G. Sek, Ghost branch photoluminescence from a polariton fluid under nonresonant excitation, Phys. Rev. Lett. **115**, 186401 (2015).
[31] F. Claude, M. J. Jacquet, R. Usciati, I. Carusotto, E. Giacobino, A. Bramati, and Q. Glorieux, High-resolution coherent probe spectroscopy of a polariton quantum fluid, Phys. Rev. Lett. **129**, 103601 (2022).
[32] T. Capelle, E. Flurin, E. Ivanov, J. Palomo, M. Rosticher, S. Chua, T. Briant, P.-F. Cohadon, A. Heidmann, T. Jacqmin, and S. Deléglise, Probing a two-level system bath via the frequency shift of an off-resonantly driven cavity, Phys. Rev. Appl. **13**, 034022 (2020).
[33] These relations are formally identical to a standard optomechanical or photon pressure system with a blue sideband pump. However, there are two differences to the usual case. First, we have a generalized susceptibility $\chi_{\mathcal{G}}$ in the equation for $\hat{c}$ with $\mathcal{G} < 0$, and secondly we have effective input noise operators $\hat{\xi}_{\mathrm{e,eff}}, \hat{\xi}_{\mathrm{i,eff}}$ with $\langle \hat{\xi}^{\dagger}_{\mathrm{eff}} \hat{\xi}_{\mathrm{eff}} \rangle = n^{\mathrm{HF}}_{\mathrm{th}} + [(\mathcal{G}-1)/\mathcal{G}](n^{\mathrm{HF}}_{\mathrm{th}}+1)$ and $\langle \hat{\xi}_{\mathrm{eff}} \hat{\xi}^{\dagger}_{\mathrm{eff}} \rangle = n^{\mathrm{HF}}_{\mathrm{th}} + 1 + [(\mathcal{G}-1)/\mathcal{G}] n^{\mathrm{HF}}_{\mathrm{th}}$ for the HF cavity with the undriven thermal bath occupation $n^{\mathrm{HF}}_{\mathrm{th}}$. This also implies that the strong drive generates a finite effective bath temperature even for $n^{\mathrm{HF}}_{\mathrm{th}} = 0$, i.e., from the cavity quantum bath.
[34] S. Gröblacher, K. Hammerer, M. R. Vanner, and M. Aspelmeyer, Observation of strong coupling between a micromechanical resonator and an optical cavity field, Nature (London) **460**, 724 (2009).
[35] J. D. Teufel, Dale Li, M. S. Allman, K. Cicak, A. J. Sirois, J. D. Whittaker, and R. W. Simmonds, Circuit cavity electromechanics in the strong-coupling regime, Nature (London) **471**, 204 (2011).
[36] J. M. Dobrindt, I. Wilson-Rae, and T. J. Kippenberg, Parametric normal-mode splitting in cavity optomechanics, Phys. Rev. Lett. **101**, 263602 (2008).
[37] J. D. Teufel, T. Donner, D. Li, J. W. Harlow, M. S. Allman, K. Cicak, A. J. Sirois, J. D. Whittaker, K. W. Lehnert, and R. W. Simmonds, Sideband cooling of micromechanical motion to the quantum ground state, Nature (London) **475**, 359 (2011).
[38] F. Massel, T. T. Heikkilä, J.-M. Pirkkalainen, S. U. Cho, H. Saloniemi, P. J. Hakonen, and M. A. Sillanpää, Microwave amplification with nanomechanical resonators, Nature (London) **480**, 351 (2011).
[39] D. Bothner, I. C. Rodrigues, and G. A. Steele, Four-wave-cooling to the single phonon level in Kerr optomechanics, Commun. Phys. **5**, 33 (2022).
[40] S. Gigan, H. R. Böhm, M. Paternostro, F. Blaser, G. Langer, J. B. Hertzberg, K. C. Schwab, D. Bäuerle, M. Aspelmeyer, and A. Zeilinger, Self-cooling of a micromirror by radiation pressure, Nature (London) **444**, 67 (2006).
[41] O. Arcizet, P.-F. Cohadon, T. Briant, M. Pinard, and A. Heidmann, Radiation-pressure cooling and optomechanical instability of a micromirror, Nature (London) **444**, 71 (2006).
[42] J. D. Teufel, J. W. Harlow, C. A. Regal, and K. W. Lehnert, Dynamical backaction of microwave fields on a nanomechanical oscillator, Phys. Rev. Lett. **101**, 197203 (2008).
[43] 10.5281/zenodo.10993590.